

First-in-human brain imaging of Alzheimer dementia patients and elderly controls with ^{18}F -MK-6240, a PET tracer targeting neurofibrillary tangle pathology

Running Title: FIH ^{18}F -MK-6240 PET in HE and AD

Authors: Talakad G. Lohith¹; Idriss Bennacef¹; Rik Vandenberghe²; Mathieu Vandebulcke²; Cristian A Salinas¹; Ruben Declercq³; Tom Reynders³; N. Florestina Telan-Choing⁴; Kerry Riffel¹; Sofie Celen⁵; Kim Serdons⁶; Guy Bormans⁵; Kuenhi Tsai⁷; Abbas Walji⁸; Eric D Hostetler¹; Jeffrey L. Evelhoch¹; Koen Van Laere⁶; Mark Forman⁹; Aubrey Stoch⁹; Cyrille Sur¹; and Arie Struyk⁹

Affiliations:

¹*Translational Biomarkers, Merck & Co., Inc., West Point, PA, USA*

²*Neurology Department, University Hospitals Leuven, Leuven, Belgium; Laboratory for Cognitive Neurology, Department of Neurosciences, KU Leuven, Leuven, Belgium; Alzheimer Research Centre KU Leuven, Leuven Institute for Neuroscience and Disease, Leuven, Belgium*

³*Translational Pharmacology Europe, Merck Sharp & Dohme Inc., Brussels, Belgium*

⁴*Translational Pharmacology Clinical Operations, Merck & Co., Inc., North Wales, PA, USA*

⁵*Radiopharmaceutical Research, KU Leuven, Leuven, Belgium*

⁶*Division of Nuclear Medicine, University Hospitals Leuven and UZ Leuven, Leuven, Belgium*

⁷*Early Clinical Statistics, Merck & Co., West Point, PA, USA*

⁸*Discovery Chemistry, Merck & Co., West Point, PA, USA*

⁹*Translational Pharmacology, Merck & Co., Inc., North Wales, PA, USA*

For correspondence or reprints contact: Arie Struyk, MD, PhD. Merck & Co., Inc. /
351 N. Sumneytown Pike | Mailstop UG4D-48 | North Wales, PA, USA 19454. Email:
arie_struyk@merck.com

First author: Talakad G. Lohith, MBBS, MMST, PhD. Merck & Co., Inc. / 770
Sumneytown Pike | Mailstop WP44D-216 | West Point, PA, USA 19486. Email:
talakad.lohith@merck.com

Financial Support: This work was sponsored by Merck & Co., Inc., Kenilworth, NJ,
USA.

Word Count: Abstract = 311; Document = 5821

ABSTRACT

^{18}F -MK-6240 is a highly selective, subnanomolar-affinity Positron Emission Tomography (PET) tracer for imaging neurofibrillary tangles (NFTs). Plasma kinetics, brain uptake, and preliminary quantitative analysis of ^{18}F -MK-6240 in healthy elderly subjects (HE), subjects with clinically probable Alzheimer disease (AD), and amnesic mild cognitive impairment (MCI) were characterized in a first-in-human study. **Methods:** Dynamic PET scans of up to 150 min were performed in 4 cognitively normal HE, 4 AD and 2 MCI subjects, after bolus injection of 152-169 MBq ^{18}F -MK-6240 to evaluate tracer kinetics and distribution in brain. Regional standardized uptake value ratio (SUVR) and distribution volume ratio (DVR) were determined using the cerebellar cortex as a reference region. Total distribution volume (V_T) was assessed by compartmental modeling using radiometabolite corrected input function in a subgroup of 6 subjects. **Results:** ^{18}F -MK-6240 had rapid brain uptake with peak standardized uptake value of 3-5, followed by a uniformly quick washout from all brain regions in HE; slower clearance was observed in regions commonly associated with NFT deposition in AD. In AD, SUVR measured between 60-90 min postinjection was high (approximately 2-4) in regions associated with NFT deposition; whereas, in HE, SUVR was approximately 1 across all brain regions suggesting high tracer selectivity for binding NFTs in vivo. ^{18}F -MK-6240 V_T was approximately 2- to 3-fold higher in neocortical and medial temporal brain regions of AD compared with HE, and stabilized by 60 min in both groups. DVR estimated by Logan reference tissue model or compartmental modeling correlated well ($R^2 > 0.9$) to $\text{SUVR}_{60-90\text{min}}$

for AD. **Conclusion:** ^{18}F -MK-6240 exhibited favorable kinetics with high-binding levels to brain regions with a plausible pattern for NFT deposition in AD. In comparison, negligible tracer binding was observed in HE. This pilot study suggests simplified ratio methods such as SUVR can be employed to quantify NFT binding. These results support further clinical development of ^{18}F -MK-6240 for potential application in longitudinal studies.

Keywords: ^{18}F -MK-6240, tau PET tracer, neurofibrillary tangles, Alzheimer disease

INTRODUCTION

Accumulation and regional spread of brain neurofibrillary tangle (NFT) pathology in Alzheimer disease (AD) progresses as a function of disease stage, presenting a target for therapeutic interventions aimed at altering disease course. A quantifiable biomarker of the magnitude and spatial distribution of NFT burden in AD subjects is accordingly an interesting tool to interrogate disease status, possessing direct relevance to therapeutic target pathology and clinical outcomes. An NFT-targeted Positron Emission Tomography (PET) radioligand is best suited for this purpose as it offers sensitive, non-invasive detection, quantification, and the potential to monitor treatment response aimed at NFTs over time in living subjects (1). Several novel PET radiotracers developed recently demonstrate plausible retention patterns for NFT pathology in the AD brain, although their specificity and sensitivity remains to be fully ascertained (2).

^{18}F -MK-6240 is a NFT-targeting PET radioligand developed by optimizing properties to deliver high binding potential (specific to non-displaceable ratio) with no off-target binding. MK-6240 showed exquisitely high binding potential to NFT pathology in vitro in human brain tissue with no evidence of displaceable signal in vivo in rhesus monkeys (3,4). Initial evaluations including radiation dosimetry studies in healthy volunteers had good safety profiles and supports further clinical investigation of ^{18}F -MK-6240 in AD subjects (manuscript in preparation).

This pilot study was designed to ascertain brain uptake and washout characteristics of ^{18}F -MK-6240 in a small, cross-sectional cohort of healthy elderly (HE) subjects and subjects diagnosed clinically with AD or mild cognitive impairment (MCI) presumptively carrying NFT pathology. Regional tracer retention was mapped to brain regions of

interest based on known neuropathological distribution of NFT across the spectrum of AD disease severity. In a subgroup of HE and AD subjects, arterial blood was sampled to quantify brain uptake relative to amount of parent radiotracer delivered to the brain.

MATERIALS AND METHODS

Subject Recruitment

The study recruited cognitively intact HE subjects (Subjects 1-4) and subjects carrying a diagnosis of either AD or MCI (Subjects 5-10). All subjects were >55 years old, with a Mini-Mental State Examination (MMSE) score of ≥ 27 for HE; an MMSE score of ≥ 26 with an objective impairment in episodic memory for MCI; and an MMSE score of ≤ 28 for subjects clinically diagnosed as probable AD by the National Institute of Neurological and Communicative Disorders and Stroke, and the Alzheimer Disease and Related Disorders Association diagnostic criteria. Active smokers were excluded from participation. Clinical diagnosis of MCI and AD was used as the sole determinant of the likelihood to carry NFT pathology; no concomitant scanning or cerebrospinal fluid (CSF) analysis for amyloid deposition was required per protocol, although for a number of subjects amyloid biomarker results were available as part of prior clinical evaluations or prior participation in clinical diagnostic studies (for further details see Table 1 and Supplemental Table 1). Per protocol, subjects were screened for medical history and underwent a physical examination, an electrocardiogram, urine analysis, laboratory blood tests (complete blood count, serum chemistries), drug screen, and pregnancy tests for females. Vital signs and electrocardiograms were recorded before the ^{18}F -MK-6240 injection, 10 and 40 min postinjection, and at the end of the scan. Urine analysis and

blood tests were repeated within 4 h of PET scan completion. Arterial blood sampling to support quantitative image analysis was performed in 3 each of HE and AD subjects who consented to arterial line placement.

The study was conducted at the University Hospital Leuven, Belgium, in conformance with principles of Good Clinical Practice. The local Ethics Committee (University Hospitals Leuven/KU Leuven), approved this study (ClinicalTrials.gov no. NCT02562989) and each subject or their legal representative (if necessary, in the case of AD or MCI subjects) signed a written informed consent before enrollment.

¹⁸F-MK-6240 Radiosynthesis

¹⁸F-MK-6240 radiosynthesis was performed as previously described with minor modifications that excluded temperature gradient during the reaction and a deprotection step (5). The radioligand had high radiochemical purity (>95%) and a molar activity of 116 ± 56 GBq/ μ mol at the time of injection (n = 10 batches).

PET Scans

Dynamic brain PET scans were acquired in 3-dimensional (3D) list mode on a Hirez Biograph 16 PET/CT camera (Siemens Medical Solutions) after a rapid (over 20 s) intravenous bolus injection of 159 ± 5 MBq (Mean \pm standard deviation [SD]; n = 10 injections) of ¹⁸F-MK-6240. The scan consisted of 2 segments from 0-90 min (segment 1) and 120-150 min (segment 2) with a 30-min break between the segments. Segment 2 was optional for AD/MCI subjects, and only Subject 5 agreed to participate. A low-dose CT was performed before each scan segment for attenuation correction. The acquisition consisted of a total of 37 frames over a period of 150 min with progressive increase in frame duration: 6×10 , 6×20 , 2×30 , 2×60 , 2×120 , 10×300 , 3×600 s (0-90 min)

and 6×300 s (120-150 min). Images were reconstructed with a standard 3D filtered-back projection algorithm including correction for scatter, attenuation, decay, random coincidences, and dead time.

Magnetic Resonance Imaging

Subjects were scanned on an Achieva 3T MR scanner (Philips Healthcare) with a 24-channel or a 32-channel head coil. The MR sequences consisted of a 3D T1-weighted Turbo Field Echo sequence, a Fluid Attenuated Inversion Recovery sequence, a diffusion-weighted imaging scan, and a Gradient Echo sequence to detect hemosiderin deposits.

Measurement of ^{18}F -MK-6240 in Plasma

To measure the radioactivity concentrations in the whole blood and plasma, arterial blood samples (2 mL each) were drawn at 10 s intervals for the first 100 s, and at approximately 2, 2.5, 3, 5, 15, 30, 45, 60, 75, and 90 min postinjection of radiotracer. Additional arterial blood samples (4 mL) were drawn at approximately 2, 5, 15, 30, 60, and 90 min postinjection of the radiotracer to measure parent ^{18}F -MK-6240 and its radioactive metabolites in the plasma, using high-performance liquid chromatography as described previously (6) with some minor modifications. One milliliter of acetonitrile was added to the plasma for protein denaturation and analysis was performed using the high-performance liquid chromatography system with 45% v/v acetonitrile in the buffered mobile phase. Ultraviolet detection was performed at 220 nm. Gamma counter lower limit of quantitation was 309 Bq.

A metabolite-corrected plasma input function was obtained as follows: the total radioactivity time course in plasma and whole blood were fitted after the peak to a

trixponential function with constant weighting. The ^{18}F -MK-6240 parent fraction in the plasma samples was fitted to a biexponential function with constant weighting. Because the parent fractions for Subject 2 had gamma counter measurement errors and measured parent fractions across time points for the other 5 subjects were similar, population-based average parent fractions from the remaining 5 subjects were used. The fitted total plasma radioactivity was multiplied by the fitted parent fraction to obtain the radiometabolite-corrected plasma input function.

Image Analysis

Image processing was performed using the PNEURO toolbox of the PMOD software package (Version 3.7, PMOD Technologies Ltd.) and SPM8 toolsets in MATLAB 2014b (MathWorks). The PET images were corrected for motion using SPM by frame-to-frame registration with the averaged PET image derived from early time frames. Subsequent processing used the PNEURO toolbox. Brain extraction with grey and white matter segmentation were performed on each subject's T1-weighted 3T magnetic resonance imaging (MRI) scan. The PET image averaged over all frames was aligned to the extracted subject MRI brain via a rigid registration algorithm, and the same transformation was then applied to the entire 0-150 min dataset. An N30R83 human brain atlas (7) was aligned to the extracted subject MRI brain via a non-linear registration algorithm. The aligned brain atlas was applied to the motion-corrected PET dynamic data to generate time-activity curves of several brain regions, including (but not limited to) the frontal cortex, parietal cortex, temporal cortex, medial temporal cortex, putamen, thalamus, cerebral white matter, and cerebellar cortex. The cortical and subcortical regions were masked for grey matter.

Regional time-activity curves as standardized uptake value (SUV) and SUV ratios (SUVR) of the target to reference region were generated over the time course of the scan, and over a scan window, during which the separation of regional SUVR curves was maximum and stable over time. Cerebellar gray matter has been reported as devoid of NFT deposition; and therefore similar to the evaluation of other tau PET tracers, we used the cerebellar cortex as reference region (8,9). Reference tissue modeling approaches such as Simplified Reference or Logan Reference Tissue Modeling (SRTM or LRTM) were performed to determine non-displaceable binding potential (BP_{ND}) for target regions (10,11). For subjects with arterial blood sampling, total volumes of distribution (V_T) were determined by compartmental modeling using an arterial input function. A 1- or 2-tissue compartment model (1-TCM, 2-TCM; reversible and irreversible versions) were selected on the basis of a model-selection metric (ie, Akaike Information Criteria). Additional tests, such as V_T time stability, were performed to determine the minimal scan length for accurate measurements and to indirectly assess the influence of radiometabolite accumulation in the brain.

Furthermore, the relationship between SUVR and distribution volume ratio (DVR) (equivalent quantity obtained as a ratio of $V_T^{target}/V_T^{reference}$ by compartmental modeling and graphical Logan plot [LGA], or as a regression slope [$BP_{ND} + 1$] by LRTM) was explored to ensure that the SUVR represented an appropriate surrogate measurement of ^{18}F -MK-6240 specific binding. The LGA and LRTM were applied to fit the equilibration start time (t^*) and the slope of the linear portion for each brain region that included data from multiple voxels within a volume-of-interest, with a maximum deviation between the regression and all measurements set to 10%.

To determine the effect of any potential defluorination-related bone uptake on adjacent cortical regions, using attenuation CT image, skull volumes-of-interest were manually delineated close to the atlas-derived temporal cortical volumes-of-interest in both HE and AD subjects, and their time-activity curves were compared.

RESULTS

A total of 4 HE, 4 AD, and 2 amnesic MCI subjects participated in this study. The subject demographics are presented in Table 1, together with CSF, beta-amyloid, and MRI biomarker data (Supplemental Table 2). Two MCI subjects were amyloid positive by PET and in 1 dementia subject, the diagnosis of AD was supported by CSF biomarkers.

The injected mass dose (mean \pm SD) of ^{18}F -MK-6240 was 0.44 ± 0.08 μg ($n = 4$ injections) in HE subjects and 0.56 ± 0.54 μg ($n = 6$ injections) in AD subjects. The ^{18}F -MK-6240 injections were well tolerated with no pharmacologic effects. Five subjects reported adverse events characterized as vascular access site bruising or site hematoma within 48 hours of dosing that were considered mild and unrelated to ^{18}F -MK-6240. No serious adverse events were reported, and no clinically significant changes in vital signs, clinical laboratory results, or electrocardiograms were observed.

Plasma Analysis

^{18}F -MK-6240 exhibited rapid metabolism following the injection with parent ^{18}F -MK-6240 in arterial plasma representing $20\% \pm 8\%$ at 15 min ($n = 5$), $10\% \pm 5\%$ at 30 min ($n = 5$), and $7 \pm 5\%$ at 90 min ($n = 5$), in HE and AD subjects (Fig. 1A). The ^{18}F -MK-6240 concentrations in arterial plasma peaked to approximately 30 SUV at 30-40 s

after tracer injection in all subjects, and then rapidly declined, followed by a slow terminal clearance (Fig. 1B).

Brain Time-Activity Curves and SUVR Analysis

Following the ^{18}F -MK-6240 injection, a high peak radioactivity uptake of 3-5 SUV occurred across brain regions in both HE and AD/MCI subjects. In HE subjects, brain uptake was followed by a rapid homogenous washout across most brain regions (Fig. 2A). By contrast, AD/MCI subjects (except Subject 5) showed higher MK-6240 retention in brain regions consistent with known NFT deposition for AD (Fig. 2B). Specifically, medial temporal lobe regions that include hippocampus, parahippocampal gyrus, and amygdala showed substantial tracer retention in 5 of 6 AD/MCI subjects. In 2 of 3 AD subjects with advanced clinical status (MMSE <20), tracer retention was also observed in temporal, frontal, and parietal neocortical regions; whereas in the third, signal was restricted to medial temporal regions bilaterally. The cerebellar cortex, a region known to be devoid of NFT deposition in AD, exhibited rapid washout similar to the brains of the HE subjects.

Representative cortical and subcortical regional uptake ratios in HE and AD subjects over time are shown (Fig. 3). Regional separation of SUVR curves between AD and HE subjects was prominent between 60-90 min with 5 of 6 AD subjects showing SUVR >1; whereas, all HE subjects had SUVR \leq 1. Therefore, SUVR regional comparisons were made by averaging over the 60-90 min scan interval following the tracer injection (Figs. 4 and 5). Of the 6 AD/MCI subjects, 3 (Subjects 8-10) showed widespread cortical and subcortical SUVR_{60-90min} of >2-3 in regions associated with AD NFT deposition. Subjects 6 and 7 showed a moderately high SUVR_{60-90min} of approximately 2, localized to the

medial temporal lobe and Subject 5 showed a focal intense signal in subcortical white matter (coronal slice; Fig. 5) near the caudate/putamen that colocalized with a hyperintense signal on a T1-weighted MRI, with $SUVR_{60-90min}$ values of approximately 1 across all other brain regions.

Brain Kinetic Analysis

As part of tracer validation to derive fully quantitative outcomes such as V_T , arterial input-based 1-TCM, 2-TCM, and LGA were performed in subjects with arterial sampling. The regional time-activity curves in HE and AD subjects were best fitted by an unconstrained, reversible 2-TCM (Fig. 6A and B). Regional V_T values (mean \pm SD) in HE subjects across cortical and subcortical regions averaged to $4.7 \pm 1.2 \text{ mL}\cdot\text{cm}^{-3}$; whereas, V_T values in AD subjects ranged from a low of $3.1 \pm 0.5 \text{ mL}\cdot\text{cm}^{-3}$ in caudate to $9.8 \pm 1.5 \text{ mL}\cdot\text{cm}^{-3}$ in the amygdala (Supplemental Fig. 1, Supplemental Tables 2 and 3).

The LGA provided linear regression slopes representing V_T with $t^* > 25$ min in both HE and AD subjects with higher slopes in NFT-associated areas of AD (Supplemental Fig. 2). The target region DVRs derived from 2-TCM and LGA corresponded well in both HE and AD subjects. The NFT-rich regions in AD subjects had values of >1 ; whereas, NFT-poor regions in AD subjects and all regions in HE subjects had values of ≤ 1 (Supplemental Tables 4 and 5). Scan data were available for up to 90 min postinjection in all subjects; therefore, the time stability of V_T was determined by analyzing truncated datasets from the 90 min scan time. The V_T values from the 60 min scan length were within 10% of terminal 90 min data in both HE and AD subjects. This could indicate that, in this small group of subjects, at least 60 min of data acquisition is

required to accurately measure V_T and that the influence of any radiometabolite accumulation for the quantification of V_T is minimal between 60-90 min (Fig. 6C).

For subjects without arterial sampling, application of an LRTM using the cerebellar cortex as a reference, yielded robust regression slopes (representing $DVR = BP_{ND} + 1$) that were higher for NFT-associated regions, such as the temporal cortex compared with other NFT-poor regions, such as the thalamus in AD subjects (Fig. 6C). The t^* values were 20-25 min across all AD subjects indicating that rapid equilibration is achieved when the slope becomes linear. The SRTM fits did not converge for all regions in HE subjects, and in most regions of AD subjects, BP_{ND} values either failed to converge or had high standard errors (data not shown).

SUVR-DVR Correlations

To support the validity of SUVR as a PET outcome measure for signal quantification in AD subjects, the SUVR values determined from the 60-90 min time window using the cerebellar cortex as reference were correlated with the DVRs obtained from 2-TCM, LGA, or LRTM and SRTM (for subjects without arterial blood sampling). Regional $SUVR_{60-90min}$ and DVRs derived from 2-TCM, LGA, and LRTM in AD subjects showed a strong linear relationship with a slope of approximately 1, supporting the validity of SUVR as a quantitative metric for signal quantification (Fig. 7, Supplemental Table 6).

DISCUSSION

This first-in-human study reports the utility of ^{18}F -MK-6240 as an NFT imaging PET tracer in a small cohort of 4 cognitively normal HE subjects, 4 subjects with clinically probable AD, and 2 subjects with amnesic MCI due to AD. We found that ^{18}F -MK-6240

exhibits regional retention in a plausible pattern for NFT pathology in AD (12). Importantly, in NFT depositing regions, signal magnitude in terms of semiquantitative SUVR or fully quantitative V_T values were higher in AD/MCI subjects compared with HE subjects, with no evidence of off-target binding in HE subjects.

In this study, images were collected dynamically up to 90 min in all subjects, and optional imaging windows from 120-150 min were collected in 3 HE subjects and 1 AD subject. In addition, arterial blood sampling for full quantitation was obtained in 3 HE and 3 AD subjects. The tracer exhibited fast plasma clearance, with only approximately 10% of the parent remaining at 30 min postinjection.

Using the cerebellar cortex as reference, SUVR curves did not always appear to reach stable values over the 30 min static window of 60-90 min, particularly in NFT-associated cortical regions of 2 AD subjects with lower MMSE scores (Fig. 3). This could be due to the slower tracer kinetics in the brain regions with a high density of NFTs in these AD subjects. In order to minimize tracer delivery effect and minimize biases introduced by measuring non-equilibrated SUVR values in high binding regions, imaging windows beyond 90 min postinjection merit further assessment. Determination of an optimal static scan time window, potentially later than 90 minutes postinjection, will be of particular importance to facilitate longitudinal assessment of tau-associated disease progression. Alternatively, different reference tissues may be explored that could provide a more appropriate stable reference for static imaging within 90 min postinjection.

The $SUVR_{60-90min}$ was approximately 1 across all NFT-rich and NFT-poor regions of the HE subjects indicating negligible off-target binding. The only region that exhibited $SUVR_{60-90min}$ values marginally >1 was the substantia nigra, although not all subjects

exhibited this elevated signal (Fig. 4). In vitro autoradiography studies carried out in brain slices of controls and AD subjects have showed no displaceable binding in the substantia nigra (13). Speculatively, the sporadic in vivo retention could be due to non-specific binding to neuromelanin, which increases with age (14). Nevertheless, this inconsistency merits further investigation in a larger cohort of subjects, as this slightly elevated signal was not observed in all subjects. In contrast, SUVR_{60-90min} values of 1.5-2 were observed in the putamen and white matter in Subjects 8 and 9 (AD) with extensive cortical spread. The presence of signal in putamen and white matter of Subjects 8 and 9 with significant cortical spread (possibly stage VI) may be specific as NFTs are present in these areas in Braak late stage (12,15). However, with other tau PET tracers similar signals have been reported for these regions not only in AD subjects but also in healthy controls, which has been attributed to off-target binding (8,16,17). Subcortical structures such as the caudate, thalamus, and brainstem showed SUVR values around 1 in both HE and AD subjects, suggesting no evidence of off-target binding and that those regions can be used as reference regions.

Two subjects diagnosed with AD did not fit the pattern of high-tracer binding with disease severity based on clinical cognition scores. Subject 5 (AD) exhibited no regional increased tracer uptake, including no tracer retention in medial temporal and limbic areas, which are generally identified as early regions of NFT accumulation (Braak I/II) (12). One area of focal uptake was observed and later identified as a hemorrhagic lesion in the putamen (visible on the coronal slice of Subject 5 in Fig. 5). Despite a clinical history suggestive of AD at the time of recruitment, subsequent clinical progression and investigations have raised questions about validity of the AD diagnosis, and scan findings

(including microhemorrhages and extensive white matter intensities) indicate a possible vascular cause to the dementia (Supplemental Table 1). However, the neuropathological diagnosis for this subject remains uncertain. A second AD subject (Subject 6) exhibited only limited medial temporal and amygdala tracer retention despite significant clinical impairment (MMSE 11), indicating a discordance between clinical stage and expected ^{18}F -MK-6240 signal based on presumptive Braak staging. The high signal localized to the amygdala is not unexpected with reports showing the presence of NFTs in amygdala in early to late stages of AD and that its signal magnitude could even be higher than in cortical regions (18,19). However, as only a small number of subjects were included in this study, conclusions regarding the specificity and the sensitivity of ^{18}F -MK-6240, as a function of disease stage and neuropathological diagnosis, cannot be drawn. One further key limitation of this study was that recruitment criteria were limited to the clinical diagnoses as an inclusionary standard and additional testing for AD pathology (eg, amyloid PET scanning or CSF analysis) was not uniformly employed. Within a number of cases, biomarker support for the diagnosis was available from prior data (Supplemental Table 1). Without biomarker support, it is possible that non-AD subjects, or subjects with concurrent, overlapping pathologies contributing to cognitive impairment, may have been part of the study sample. Future investigation with larger, better-defined, cross-sectional subject cohorts undergoing serial PET scanning over time, as well as correlating the PET signal to postmortem pathologic detection of NFTs in same subject, will help clarify the relationship between tracer retention and clinical progression.

The kinetic analysis resulted in a reversible 2-TCM better describing the tracer kinetics across regions in all subjects, indicating the presence of specific and non-displaceable tissue compartments. For reference-tissue modeling, the LRTM provided stable estimates across all subjects. The correlation between SUVR and DVRs obtained from 2-TCM, LGA, or LRTM was robust (Fig. 7, Supplemental Table 6), but further validation in more subjects is required to ascertain the use of SUVR to quantify the ^{18}F -MK-6240 signal. The exploratory SRTM analysis was problematic in this small sample with respect to convergence issues and high BP_{ND} errors (data not shown). A larger sample will help to clarify the nature of these issues.

Regarding defluorination, a concern for some ^{18}F -labeled tracers, examination of the ^{18}F -MK-6240 scans indicate that HE subjects had a low-level signal on the skull that was slightly higher compared with adjacent cortical signal at late time points (Supplemental Fig. 3A). Importantly, the cortical and subcortical signals in HE subjects were not affected by the presence of low-level skull signal as evidenced by SUVRs of cortical and putamen SUVRs plateauing at 1; whereas, bone SUVR continue to rise over time (Supplemental Fig. 3B). By contrast, AD subjects showed prominent cortical signal with higher SUVR over time because of tau-associated NFT signal that can impact the clearance kinetics in cortical regions. It should be noted that because of partial volume effects, the low-level skull signal could be affected by the adjacent higher cortical signal. The subcortical putamen SUVR however plateaued at 1 (Supplemental Fig. 3C).

CONCLUSION

In this first-in-human study, in a limited number of subjects, ^{18}F -MK-6240 produced robust PET signals in regions plausibly associated with NFT deposition in AD subjects and nominal signals in HE subjects. Associations between DVR and SUVR measurements had minimal bias suggesting that in vivo NFT deposition can be reasonably quantified using SUVR. Further studies evaluating longer dynamic scan duration for detecting the optimal static time window, test-retest scans to characterize reproducibility measures for longitudinal NFT signal changes, and arterial sampling based kinetic modeling in multiple subjects are warranted to better understand ^{18}F -MK-6240 SUVR bias, relative to more quantitative outcomes.

DISCLOSURES

The Leuven University (UZ Leuven) groups obtained financial sponsoring from Merck & Co, Inc., Kenilworth, NJ, USA, for the human PET study. C. Sur, A. Struyk, TG. Lohith, I. Bennacef, R. Declercq, T. Reynders, NF. Telan-Choing, A. Walji, ED. Hostetler, JL. Evelhoch, M. Forman, K. Riffel, and A. Stoch are employees of Merck Sharp & Dohme Corp., a subsidiary of Merck & Co., Inc., Kenilworth, NJ USA, who may own stock and/or hold stock options in the Company. CA Salinas and K Tsai were employees of Merck Sharp & Dohme Corp., a subsidiary of Merck & Co., Inc., Kenilworth, NJ, USA, at the time of the study. KU Leuven Research & Development has material transfer agreements (R. Vandenberghe as principal investigator) with Avid Radiopharmaceuticals, Piramal Imaging, and Tohoku University. UZ Leuven has clinical

trial agreements (R. Vandenberghe as principal investigator) with Abbvie, Biogen, GE Healthcare, Eli Lilly, MSD, Novartis, and Roche. R. Vandenberghe is the principal investigator of the pivotal ^{18}F -flutemetamol Phase 1 and 2 studies. No other potential conflicts of interest relevant to this article exist.

ACKNOWLEDGEMENTS

The authors thank the staff of the Memory Clinic and of the Nuclear Medicine Department of the University Hospital Leuven including study nurses Carine Schildermans and Kwinten Porters, for their contribution in conducting the study. Editorial assistance was provided by Michele Durocher of ExecuPharm, King of Prussia, PA, USA. This assistance was funded by Merck Sharp & Dohme Corp., a subsidiary of Merck & Co., Inc., Kenilworth, NJ, USA. The authors sincerely thank the healthy volunteers, AD/MCI subjects, and their families for their participation in the study.

REFERENCES

1. Villemagne VL, Fodero-Tavoletti MT, Masters CL, Rowe CC. Tau imaging: early progress and future directions. *Lancet Neurol.* 2015;14:114-124.
2. Dani M, Edison P, Brooks DJ. Imaging biomarkers in tauopathies. *Parkinsonism Relat Disord.* 22 Suppl 1:S26-28.
3. Walji AM, Hostetler ED, Selnick H, et al. Discovery of 6-(Fluoro-(18)F)-3-(1H-pyrrolo[2,3-c]pyridin-1-yl)isoquinolin-5-amine ([18F]-MK-6240): a positron emission tomography (PET) imaging agent for quantification of neurofibrillary tangles (NFTs). *J Med Chem.* 2016;59:4778-4789.
4. Hostetler ED, Walji AM, Zeng Z, et al. Preclinical characterization of ¹⁸F-MK-6240, a promising PET tracer for in vivo quantification of human neurofibrillary tangles. *J Nucl Med.* 2016;57:1599-1606.
5. Collier TL, Yokell DL, Livni E, et al. cGMP production of the radiopharmaceutical [(18)F]MK-6240 for PET imaging of human neurofibrillary tangles. *J Labelled Comp Radiopharm.* 2017;60:263-269.
6. Joshi AD, Sanabria-Bohorquez SM, Bormans G, et al. Characterization of the novel GlyT1 PET tracer [18F]MK-6577 in humans. *Synapse.* 2015;69:33-40.
7. Hammers A, Allom R, Koepp MJ, et al. Three-dimensional maximum probability atlas of the human brain, with particular reference to the temporal lobe. *Hum Brain Mapp.* 2003;19:224-247.
8. Chien DT, Bahri S, Szardenings AK, et al. Early clinical PET imaging results with the novel PHF-tau radioligand [F-18]-T807. *J Alzheimers Dis.* 2013;34:457-468.
9. Kimura Y, Ichise M, Ito H, et al. PET quantification of tau pathology in human brain with 11C-PBB3. *J Nucl Med.* 2015;56:1359-1365.
10. Logan J, Fowler JS, Volkow ND, Wang GJ, Ding YS, Alexoff DL. Distribution volume ratios without blood sampling from graphical analysis of PET data. *J Cereb Blood Flow Metab.* 1996;16:834-840.
11. Salinas CA, Searle GE, Gunn RN. The simplified reference tissue model: model assumption violations and their impact on binding potential. *J Cereb Blood Flow Metab.* 2015;35:304-311.
12. Braak H, Alafuzoff I, Arzberger T, Kretschmar H, Del Tredici K. Staging of Alzheimer disease-associated neurofibrillary pathology using paraffin sections and immunocytochemistry. *Acta Neuropathol.* 2006;112:389-404.

13. Zeng Z, Miller PJ, Connolly BM, et al. In vitro binding studies to evaluate the NFT-specificity of [³H]MK-6240 and [³H]AV-1451 binding in subcortical regions of the human AD brain. *Alzheimers Dement*. 2017;P150-P151.
14. Zecca L, Bellei C, Costi P, et al. New melanic pigments in the human brain that accumulate in aging and block environmental toxic metals. *Proc Natl Acad Sci U S A*. 2008;105:17567-17572.
15. Braak H, Braak E. Staging of Alzheimer's disease-related neurofibrillary changes. *Neurobiol Aging*. 1995;16:271-278.
16. Marquie M, Normandin MD, Vanderburg CR, et al. Validating novel tau positron emission tomography tracer [F-18]-AV-1451 (T807) on postmortem brain tissue. *Ann Neurol*. 2015;78:787-800.
17. Ng KP, Pascoal TA, Mathotaarachchi S, et al. Monoamine oxidase B inhibitor, selegiline, reduces 18F-THK5351 uptake in the human brain. *Alzheimers Res Ther*. 2017;9:25.
18. Nelson PT, Abner EL, Patel E, et al. The amygdala as a locus of pathologic misfolding in neurodegenerative diseases. *J Neuropathol Exp Neurol*. 2018;77:2-20.
19. Nelson PT, Abner EL, Scheff SW, et al. Alzheimer's-type neuropathology in the precuneus is not increased relative to other areas of neocortex across a range of cognitive impairment. *Neurosci Lett*. 2009;450:336-339.

FIGURES

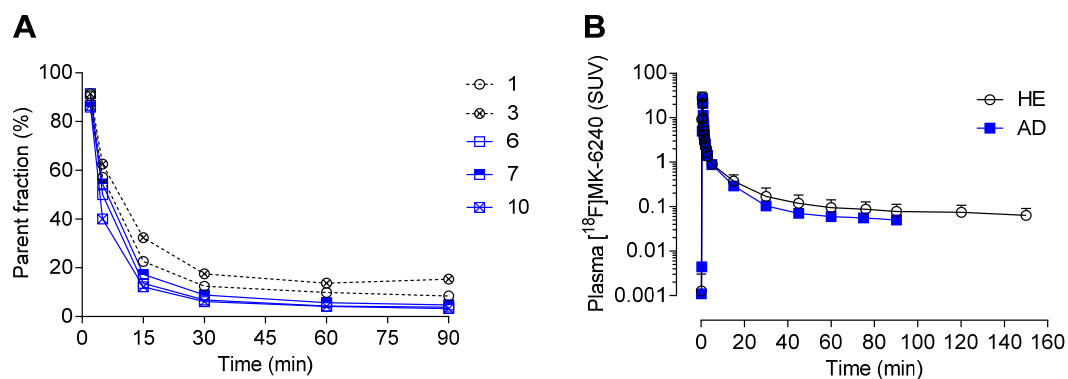


FIGURE 1. (A) ^{18}F -MK-6240 parent fraction in HE and AD subjects. (B) Time course of parent ^{18}F -MK-6240 concentrations in arterial plasma of HE and AD subjects (Mean \pm SD, n = 3). Parent ^{18}F -MK-6240 concentrations in arterial plasma for HE Subject 2 was derived using average parent fraction from remaining 5 subjects (see Methods Section for details).

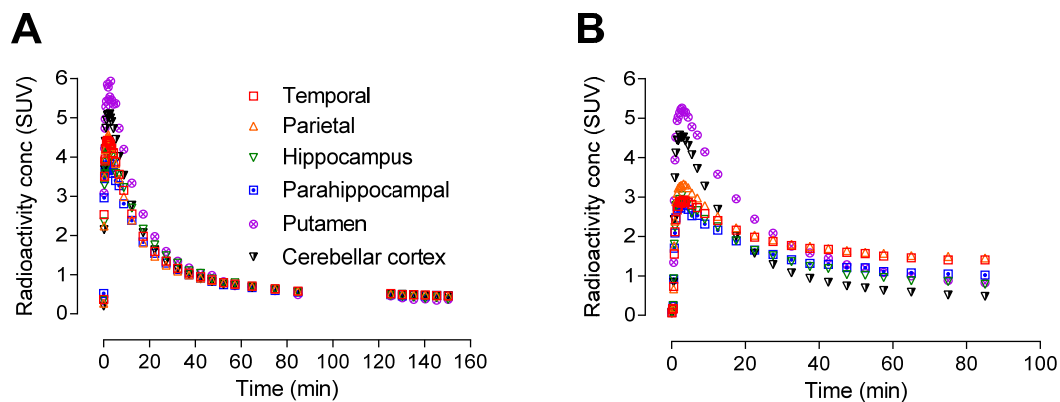


FIGURE 2. Regional brain radioactivity concentration time course in a representative, Subject 2 (HE; A), and Subject 8 (AD; B) after intravenous injection of ^{18}F -MK-6240. Note: HE subject was scanned for 150 min, and AD subject for 90 min postinjection of the radiotracer.

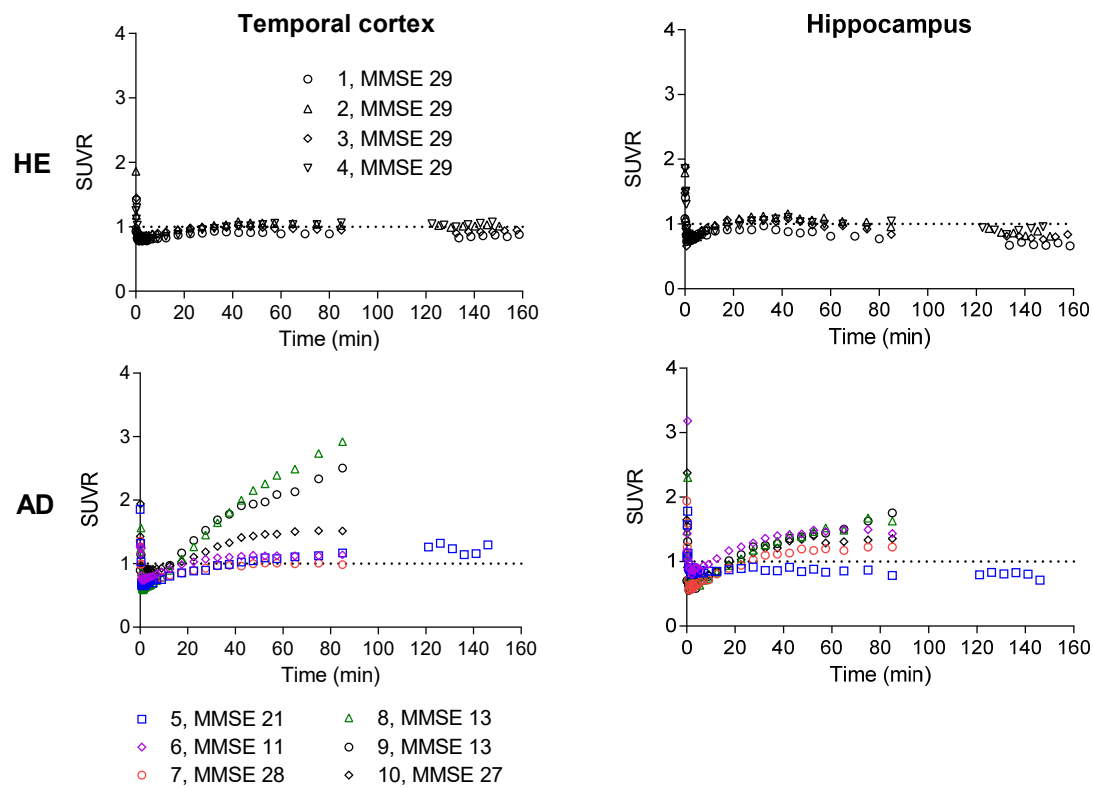


FIGURE 3. Regional (representative cortical and subcortical) SUVR time course with the cerebellar cortex as reference.

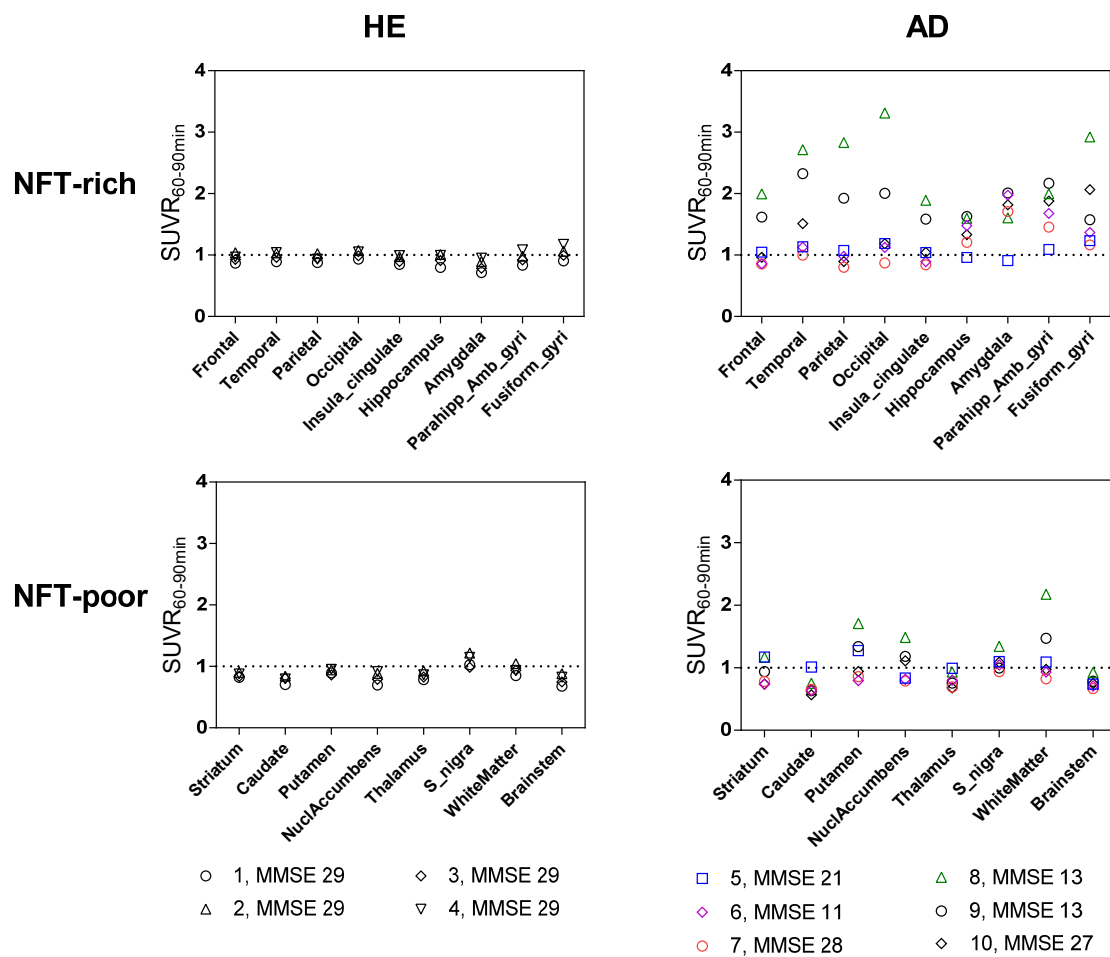


FIGURE 4. Regional $SUVR_{60-90 \text{ min}}$ with cerebellar cortex as a reference across brain regions expected to be NFT-rich and NFT-poor.

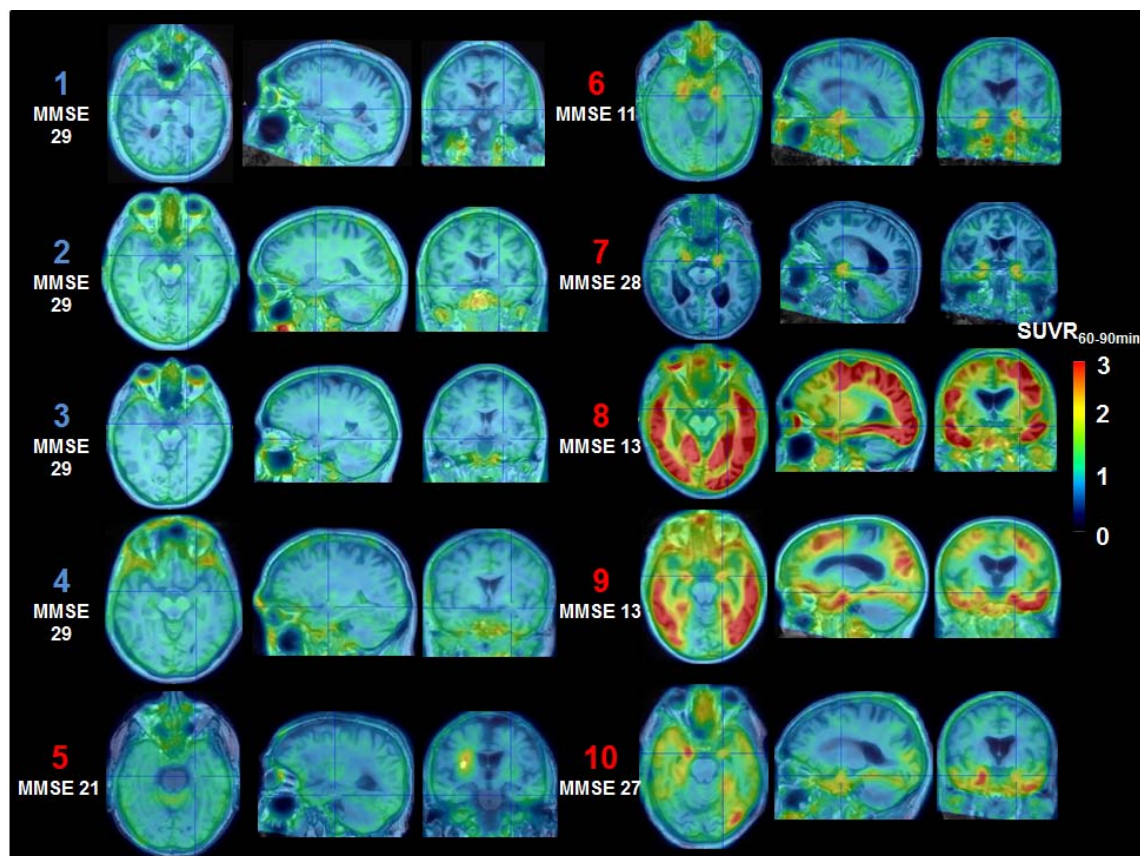


FIGURE 5. ¹⁸F-MK-6240 PET fused to individual T1-weighted MRI images for 4 HE (Subjects 1-4) and 6 AD/MCI (Subjects 5-10). The PET images are averaged between 60-90 min scan time, at the level of the medial temporal cortex, and scaled as SUVR with cerebellar cortex as a reference region. An identical rainbow color scale of 0-3 is shown to compare the tracer distribution between subjects.

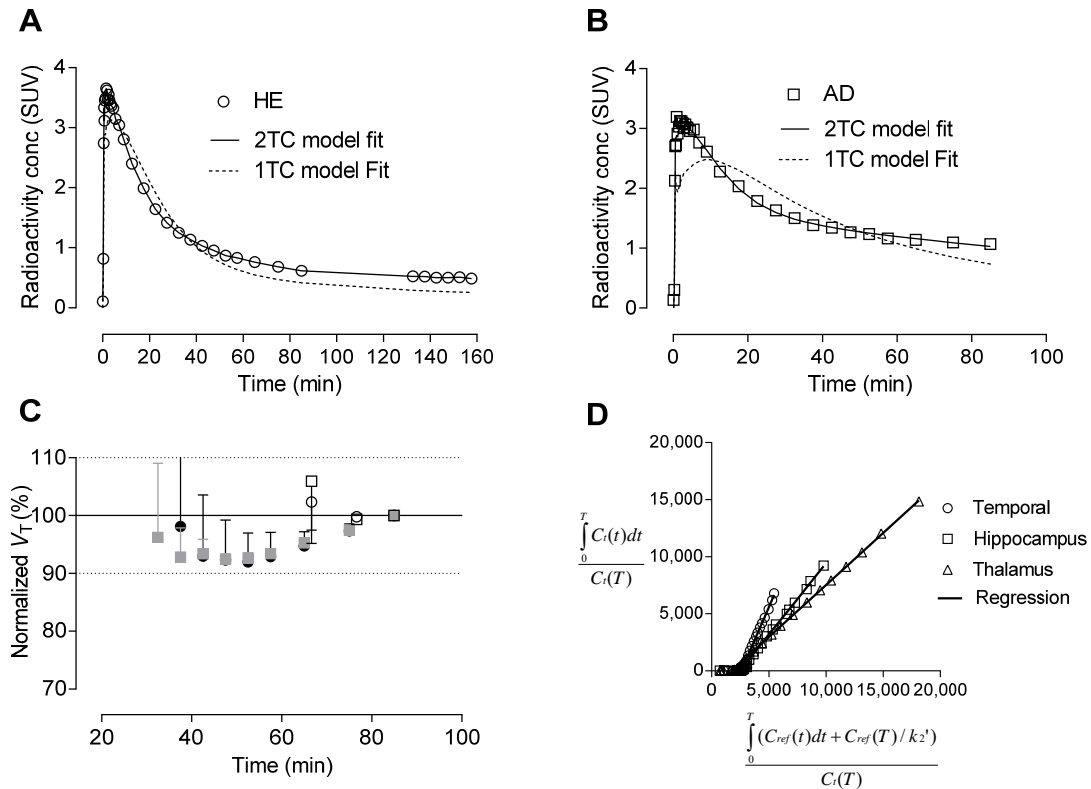


FIGURE 6. Time-activity curves with 1-TCM and 2-TCM fits for the temporal cortex from a cognitively HE subject (1; A) and an AD subject (10; B). (C) Time-stability of V_T calculated for cerebellar cortex (circles) and temporal cortex (squares) in HE (open symbols) and AD subjects (filled symbols) using unconstrained 2-TCM with increasingly truncated acquisition times up to 30 min postinjection. Values are normalized as percentage of terminal value obtained from the 90 min scan (mean \pm SD, $n = 3$). (D) Regional Logan plots (open symbols) and linear regressions (solid lines) derived from the LRTM with cerebellar cortex as a reference region in a representative AD subject (Subject 8) with no arterial sampling. Linear regression was applied after a real time (t^*) of 15

min. Regression line slopes representing DVRs for temporal cortex, hippocampus, and thalamus were 2.31, 1.25, and 0.91, respectively.

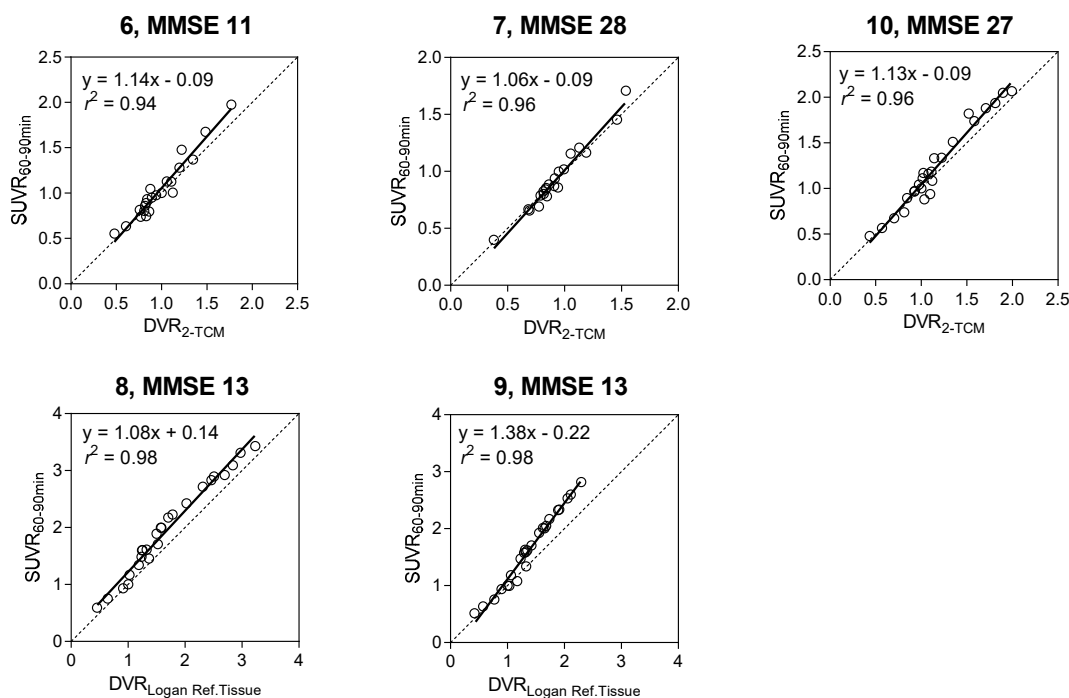


FIGURE 7. Relationship between SUVR and DVR measures in AD subjects. Top row shows the correlation between SUVR_{60-90min} and DVR measured by a 2-tissue compartment model in 3 subjects with arterial blood sampling. Bottom row shows correlation between SUVR_{60-90min} and DVR measured by Logan reference tissue model in 2 subjects without arterial blood sampling. Subject 5 was excluded, as there was minimal to no ¹⁸F-MK-6240 signal in the brain. Linear regression lines are plotted for all subjects.

TABLES

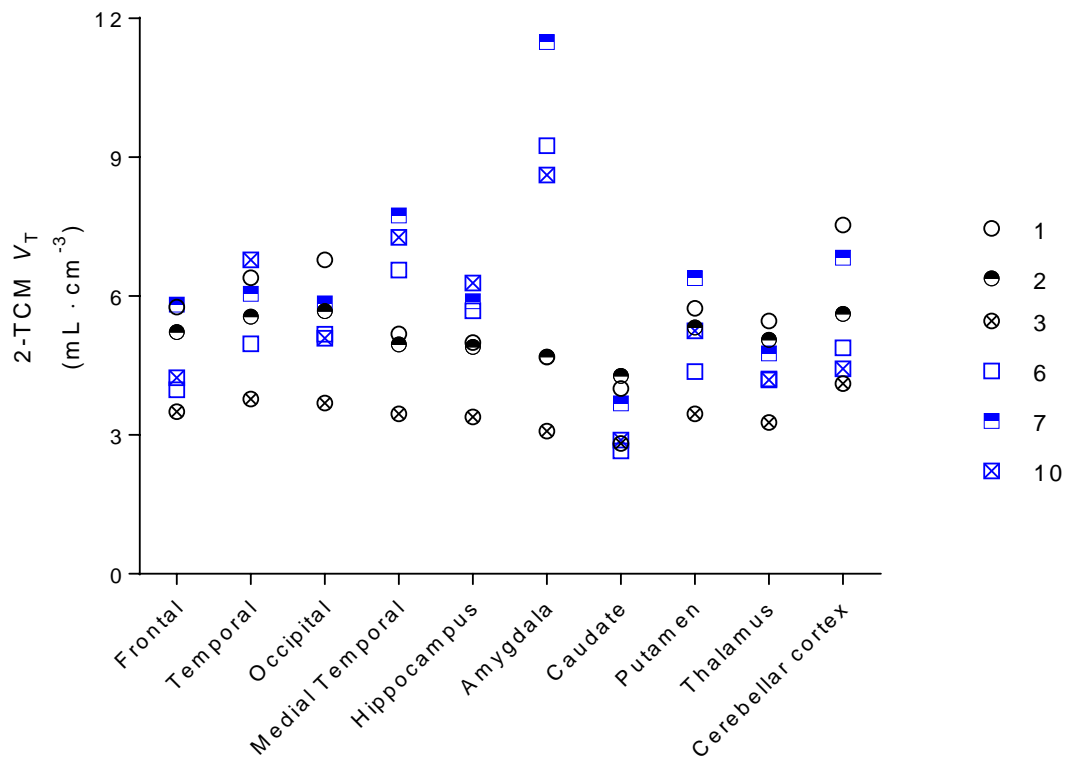
TABLE 1
Demography

Subject	Gender	Age (Years)	Clinical Diagnosis	MMSE	Dose (MBq)	Arterial Sampling	Amyloid PET
HE							
1	F	59	HE	29	161	+	N/A
2	M	66	HE	29	153	+	N/A
3	M	68	HE	29	155	+	N/A
4	M	72	HE	29	152	-	- ve
AD/MCI							
5	M	75	AD	21	169	-	N/A
6	M	67	AD	11	160	+	N/A
7	M	74	MCI	28	162	+	+ ve
8	M	74	AD	13	163	-	N/A
9	F	70	AD	13	157	-	N/A
10	M	80	MCI	27	158	+	+ ve

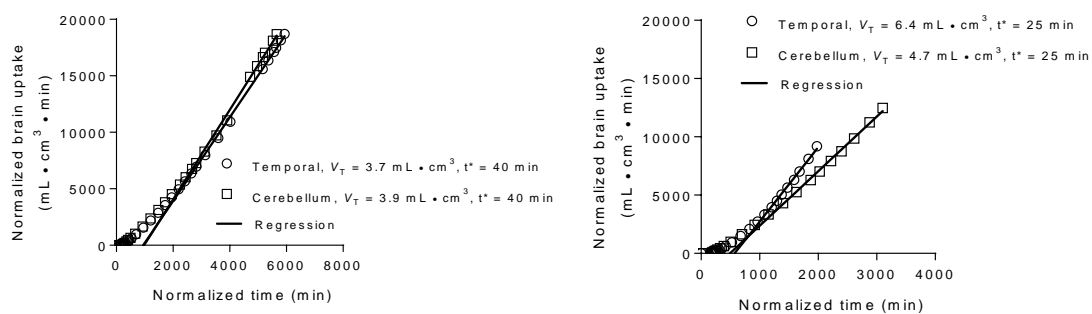
MMSE = Mini-Mental State Examination, Amyloid PET = ^{18}F -florbetaben or ^{18}F -flutemetamol amyloid PET scan supporting AD diagnosis, HE = healthy elderly, N/A = not available, AD = clinically probable Alzheimer disease, MCI = amnesic mild cognitive impairment. Additional diagnostic details about the CSF, PET, and MRI results are provided in Supplemental Table 1.

SUPPLEMENTAL DATA

SUPPLEMENTAL FIGURES

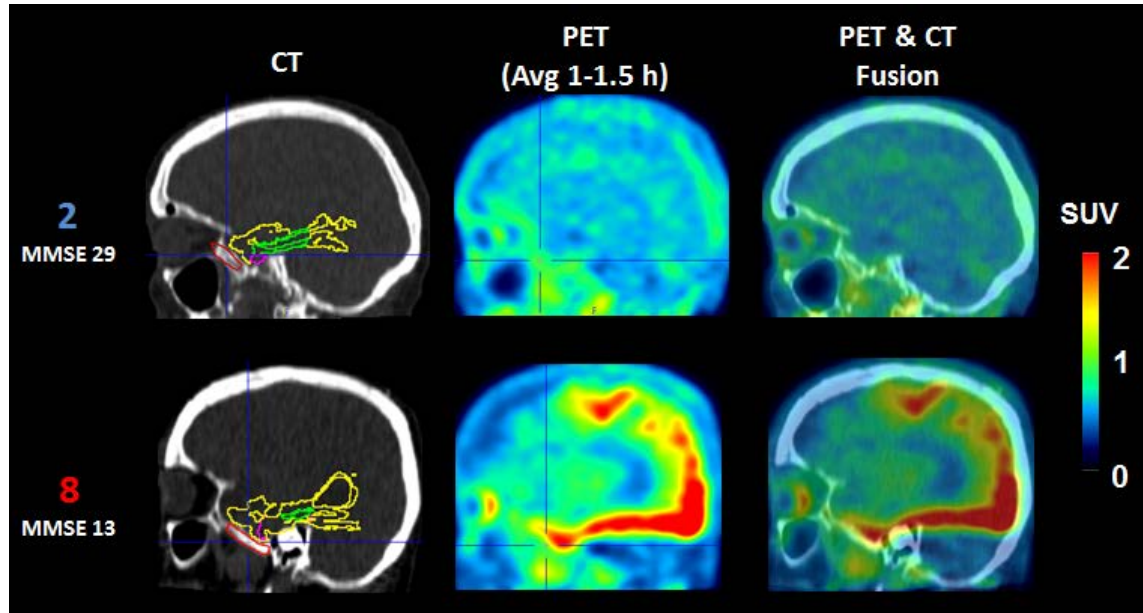


SUPPLEMENTAL FIGURE 1. Comparison of total V_T in various brain regions between cognitively HE subjects (1, 2, and 3) and AD subjects (6, 7, and 10) who received arterial sampling. V_T values were calculated using unconstrained 2-tissue compartmental model (2-TCM).

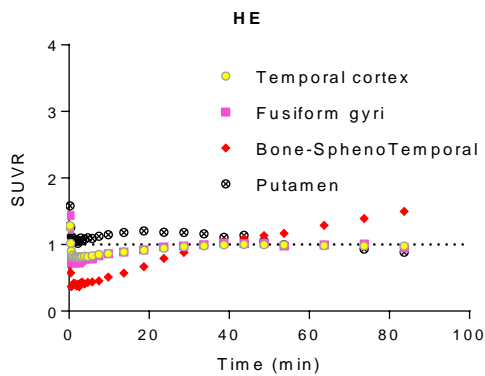


SUPPLEMENTAL FIGURE 2. Regional Logan plots (open symbols) and linear regressions (solid lines) derived from invasive Logan plot in a representative HE (Subject 3 – left plot) and AD (Subject 10 – right plot). Normalized time on x-axis is derived by the equation: $\int_0^T C_p(t)dt/C_t(T)$. Normalized brain uptake on y-axis is derived by the equation: $\int_0^T C_t(t)dt/C_t(T)$.

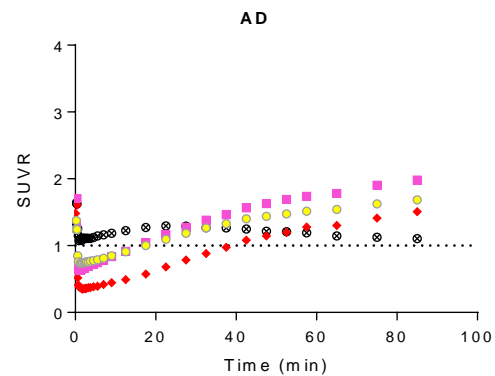
A



B



C



SUPPLEMENTAL FIGURE 3. Effect of bone uptake due to potential defluorination on brain cortical uptake. (A) Sagittal cross-sectional images (CT, PET, and PET and CT fusion) of a representative HE (2) subject and AD (8) subject showing atlas-derived regional VOI overlays (temporal cortex in yellow, fusiform gyri in pink, parahippocampal gyri in green) and manually drawn speno-temporal bone VOIs (in red). PET images are averaged between 60-90 min and are color scaled as SUV between 0 and 2. (B) Regional (Brain cortices,

adjacent bone, and putamen) SUVR time course in HE subjects with cerebellar cortex as a reference. Curves represent a mean of 4 subjects. (C) Regional (Brain cortices, adjacent bone, putamen) SUVR time course in AD subjects with cerebellar cortex as reference. Curves represent a mean of 6 subjects.

SUPPLEMENTAL TABLES

SUPPLEMENTAL TABLE 1: CSF, Amyloid PET, and MRI characteristics in AD cohort

Subject ID	Clinical diagnosis	CSF			Amyloid PET		MRI		
		A β 42 (>853 pg/mL)	Total tau (<400 pg/mL)	¹⁸¹ phosphotau (<65 pg/mL)	(SUVR <1.29)		MTA R	MTA L	ARWMC
5	Dementia	439	163	29.4	N/A	2	2	3	8
6	Dementia	N/A	N/A	N/A	N/A	0	1	1	1
7	MCI	707	496	66	1.73	3	3	0	0
8	Dementia	409	1042	164	N/A	3	3	1	0
9	Dementia	N/A	N/A	N/A	N/A	2	3	0	0
10	MCI	782	1336	165	1.71	2	3	0	0

ARWMC = Age-related white matter change (based on reference 1), CSF = Cerebrospinal fluid (cutoff criteria based on reference 2), GRE = Gradient recalled echo, MCI = Mild cognitive impairment, MTA R/L= Medial temporal lobe atrophy score (based on reference 3) right/left, N/A = not applicable, SUVR = Regional standard uptake value ratio. The values between brackets indicate the normal range. The amyloid PET was performed using ¹⁸F-florbetaben.

SUPPLEMENTAL TABLE 2: Rate constants and total distribution volumes from two-tissue compartment model in HE subjects

Brain region	Two-tissue compartmental rate constants								Two-tissue V_T (mL • cm ⁻³)			
	K_1 (mL • cm ⁻³ • min ⁻¹)		k_2 (min ⁻¹)		k_3 (min ⁻¹)		k_4 (min ⁻¹)					
Temporal	0.326	(1.2%)	0.135	(2.1%)	0.012	(6.5%)	0.012	(8.4%)	5.2	±	1.3	(2.2%)
Hippocampus	0.283	(1.5%)	0.115	(3%)	0.012	(11.3%)	0.017	(12.3%)	4.4	±	0.9	(2.2%)
Amygdala	0.286	(2.5%)	0.108	(4.6%)	0.008	(18.2%)	0.013	(23.4%)	4.2	±	0.9	(4%)
Caudate	0.274	(1.6%)	0.120	(3.1%)	0.012	(14.1%)	0.016	(12.1%)	3.7	±	0.8	(2%)
Putamen	0.417	(1.3%)	0.124	(2.9%)	0.010	(17.2%)	0.023	(14%)	4.8	±	1.2	(1.4%)
Cerebellar cortex	0.349	(1.2%)	0.143	(2%)	0.010	(6%)	0.010	(9.3%)	5.8	±	1.7	(2.8%)

Rate constants are presented as median values and V_T values as mean ± SD from 3 subjects. For each brain region, median standard errors are listed in parentheses and are expressed as % of the variable itself.

SUPPLEMENTAL TABLE 3: Rate constants and total distribution volumes from two-tissue compartment model in AD subjects

Brain region	Two-tissue compartmental rate constants				Two-tissue V_T (mL • cm ⁻³)
	K_1 (mL • cm ⁻³ • min ⁻¹)	k_2 (min ⁻¹)	k_3 (min ⁻¹)	k_4 (min ⁻¹)	
Temporal	0.336 (1.1%)	0.144 (2.2%)	0.022 (4.1%)	0.015 (5.2%)	5.9 ± 0.9 (2%)
Hippocampus	0.267 (1.8%)	0.117 (4.5%)	0.033 (8.2%)	0.018 (8.4%)	6.0 ± 0.3 (2.9%)
Amygdala	0.234 (2.3%)	0.103 (5.9%)	0.035 (9.1%)	0.011 (13.9%)	9.8 ± 1.5 (6.6%)
Caudate	0.233 (2.5%)	0.141 (5.3%)	0.021 (13.2%)	0.023 (10.5%)	3.1 ± 0.5 (2.1%)
Putamen	0.470 (1.2%)	0.145 (2.8%)	0.021 (9.2%)	0.034 (6.7%)	5.3 ± 1.0 (1%)
Cerebellar cortex	0.335 (0.9%)	0.145 (1.7%)	0.017 (4.6%)	0.016 (6.4%)	5.4 ± 1.3 (1.7%)

Rate constants are presented as median values and V_T values as mean ± SD from three subjects. For each brain region, median standard errors are listed in parentheses and are expressed as % of the variable itself.

SUPPLEMENTAL TABLE 4: SUVRs and DVRs from different models in HE subjects

Brain region	SUVR_{60-90 min}	DVR_{2-TCM}	DVR_{Logan Plot}	DVR_{LoganRefTissue}
Temporal	0.98 ± 0.07	0.88 ± 0.08	0.92 ± 0.06	0.94 ± 0.04
Hippocampus	0.93 ± 0.10	0.76 ± 0.12	0.82 ± 0.09	0.91 ± 0.07
Amygdala	0.84 ± 0.11	0.70 ± 0.08	0.75 ± 0.09	0.84 ± 0.07
Caudate	0.79 ± 0.06	0.67 ± 0.10	0.70 ± 0.07	0.79 ± 0.04
Putamen	0.91 ± 0.04	0.84 ± 0.11	0.89 ± 0.06	1.01 ± 0.06

DVR_{2TCM} and DVR_{Logan Plot} values are Mean ± SD from n = 3 HE subjects, whereas SUVR_{60-90 min} and DVR_{LoganRefTissue} are from n = 4

HE subjects

SUPPLEMENTAL TABLE 5: SUVRs and DVRs from different models in AD subjects

Brain region	SUVR_{60-90 min}	DVR_{2TCM}	DVR_{Logan Plot}	DVR_{LoganRefTissue}
Temporal	1.64 ± 0.72	1.12 ± 0.21	1.12 ± 0.22	1.39 ± 0.57
Hippocampus	1.37 ± 0.25	1.16 ± 0.05	1.20 ± 0.13	0.99 ± 0.50
Amygdala	1.67 ± 0.40	1.61 ± 0.14	1.73 ± 0.15	1.20 ± 0.60
Caudate	0.71 ± 0.16	0.62 ± 0.06	0.65 ± 0.08	0.68 ± 0.10
Putamen	1.15 ± 0.35	0.97 ± 0.12	1.03 ± 0.08	1.19 ± 0.20

DVR_{2TCM} and DVR_{Logan Plot} values are Mean ± SD from n = 3 AD subjects, whereas SUVR_{60-90 min} and DVR_{LoganRefTissue} are from n = 6 AD subjects

SUPPLEMENTAL TABLE 6: Correlations between SUVR and DVRs across subjects

Subject	SUVR _{60-90min} vs. DVR _{2-TCM}			SUVR _{60-90min} vs. DVR _{Logan Plot}			SUVR _{60-90min} vs. DVR _{Logan Ref.Tissue}		
	R ²	Slope	Intercept	R ²	Slope	Intercept	R ²	Slope	Intercept
1	0.61	0.64	0.39	0.78	0.8	0.21	0.88	1.18	-0.17
2	0.54	0.80	0.29	0.65	1.01	0.06	0.5	1.02	0
3	0.77	0.99	0.05	0.78	0.86	0.17	0.63	1.07	-0.08
4	N/A	N/A	N/A	N/A	N/A	N/A	0.31	0.9	0.14
5	N/A	N/A	N/A	N/A	N/A	N/A	0.85	1.17	-0.01
6	0.94	1.14	-0.09	0.95	1.13	-0.12	0.83	1.47	-0.44
7	0.96	1.06	-0.09	0.94	1	0	0.79	1.36	-0.29
8	N/A	N/A	N/A	N/A	N/A	N/A	0.98	1.08	0.14
9	N/A	N/A	N/A	N/A	N/A	N/A	0.98	1.38	-0.22
10	0.96	1.13	-0.09	0.96	1.11	-0.08	0.9	1.51	-0.45

N/A: Not applicable due to no arterial sampling.

SUPPLEMENTAL REFERENCES

1. Wahlund LO, Barkhof F, Fazekas F, et al. A new rating scale for age-related white matter changes applicable to MRI and CT. *Stroke*. Jun 2001; 32(6):1318-1322.
2. Adamczuk K, Schaefferbeke J, Vanderstichele HM, et al. Diagnostic value of cerebrospinal fluid A β ratios in preclinical Alzheimer's disease. *Alzheimers Res Ther*. Dec 2015; 18;7(1):75.
3. Scheltens P, Weinstein HC, Leys D. Neuro-imaging in the diagnosis of Alzheimer's disease. I. Computer tomography and magnetic resonance imaging. *Clin Neurol Neurosurg*. 1992;94(4):277-289.



The Journal of
NUCLEAR MEDICINE

First-in-human brain imaging of Alzheimer dementia patients and elderly controls with ^{18}F -MK-6240, a PET tracer targeting neurofibrillary tangle pathology

Talakad G Lohith, Idriss Bennacef, Rik Vandenberghe, Mathieu Vandebulcke, Cristian Salinas-Valenzuela, Ruben Declercq, Tom Reynders, Florestina Telan-Choing, Kerry Riffel, Sofie Celen, Kim Serdons, Guy Bormans, Kuenhi Tsai, Abbas Walji, Eric D. Hostetler, Jeffrey L. Evelhoch, Koen Van Laere, Mark Forman, Aubrey Stoch, Cyrille Sur and Arie Struyk

J Nucl Med.

Published online: June 7, 2018.

Doi: 10.2967/jnumed.118.208215

This article and updated information are available at:

<http://jnm.snmjournals.org/content/early/2018/06/06/jnumed.118.208215>

Information about reproducing figures, tables, or other portions of this article can be found online at:

<http://jnm.snmjournals.org/site/misc/permission.xhtml>

Information about subscriptions to JNM can be found at:

<http://jnm.snmjournals.org/site/subscriptions/online.xhtml>

JNM ahead of print articles have been peer reviewed and accepted for publication in *JNM*. They have not been copyedited, nor have they appeared in a print or online issue of the journal. Once the accepted manuscripts appear in the *JNM* ahead of print area, they will be prepared for print and online publication, which includes copyediting, typesetting, proofreading, and author review. This process may lead to differences between the accepted version of the manuscript and the final, published version.

The Journal of Nuclear Medicine is published monthly.
SNMMI | Society of Nuclear Medicine and Molecular Imaging
1850 Samuel Morse Drive, Reston, VA 20190.
(Print ISSN: 0161-5505, Online ISSN: 2159-662X)

© Copyright 2018 SNMMI; all rights reserved.

The logo for the Society of Nuclear Medicine and Molecular Imaging (SNMMI) consists of the letters 'S', 'N', 'M', and 'I' arranged in a 2x2 grid. Each letter is white and set within a red square. To the right of this grid, the full name of the society is written in a sans-serif font: 'SOCIETY OF NUCLEAR MEDICINE AND MOLECULAR IMAGING'.

SOCIETY OF
NUCLEAR MEDICINE
AND MOLECULAR IMAGING